Annual Methodological Archive Research Review
http://amresearchreview.com/index.php/Journal/about
Volume 3, Issue 10 (2025)

Online ISSN 3007-3197
Print ISSN 3007-3189

http://amresearchreview.com/index.php/Journal/about

Synthesis of Cr M-type Hexagonal Ferrites by Sol-Gel Auto-Combustion Methods

Saima khalid
Department of Basic Sciences, Superior University Lahore
Email: su92-mpphw-f23-001@superior.edu.pk

ABSTRACT

The basic formula of contaminant M-type hexagonal Ferrites is $Ca_{0.25}Ba_{0.75}Cr_xFe_{12-2x}O_{19}$, where x=(0.0, 0.05,0.10, 0.15, and 0.20) was synthesized by using sol-gel auto combustion method. X-ray diffraction (XRD) analysis was employed to determine the geometry of single-phase Cr hexaferrite. We investigated the structural, morphological, or dielectric characteristics. The samples were sintered at 1200°C for 8 hours. The Single-phase magneto plumbite form is revealed by the XRD analysis. The basic purpose of $Ca_{0.25}Ba_{0.75}Cr_xFe_{12-x}O_{19}$ hexaferrites, including lattice parameters (a or c), crystallite size, and cell volume $V(Å)^3$, was assessed. The particle's crystallite size ranged from 45.85 to 42.96 nm. SEM analysis of the samples indicates a consistent platelet hexagonal shape and uniform distribution of all the grains. The materials morphological appearance as seen by using a scanning electron microscope (SEM), whereas microscopy displays uniformly scattered particles and a uniform platelets hexagonal shape. The rule for approximation towards the saturation magnetization (H_C) has been employed to explore saturation magnetization and magneto crystalline anisotropic. These produced samples such as quality factor(Q-values), ac conductivity, dielectric constant(έ), dielectric loss(ε″), tangent loss(tanδ) have also been studied. Such observed dielectric features were useful for greater applications like microwave absorber, voltage controlled, dielectric resonator and recording medium.

Introduction

Modern devices such as televisions, cellular phones, microwaves, radar systems, and other wireless technologies commonly operate within the ultra-high frequency (UHF) bands, spanning frequencies from 3 MHz to 3 GHz. The trend toward miniaturization of these devices necessitates the development of materials with enhanced magnetic and dielectric properties to support smaller, more efficient antennas. Electromagnetic interference (EMI) and electromagnetic radiation (EMR) have become significant challenges in communication technologies due to the proliferation of smart devices. To address these issues, advanced multifunctional ferrite materials are under extensive investigation[1, 2].

Among magnetic materials, hexagonal ferrites, or hexaferrites, have gained considerable attention due to their excellent physical and chemical properties[3-5]. These ferrites are widely used in everyday applications owing to their cost-effectiveness, chemical stability, and uniaxial magnetic anisotropy[5, 6]. Notably,

Annual Methodological Archive Research Review
http://amresearchreview.com/index.php/Journal/about
Volume 3, Issue 10 (2025)

Online ISSN 3007-3197
Print ISSN 3007-3189
http://amresearchreview.com/index.php/Journal/about

barium hexaferrite (BaM) constitutes over half of the global hexaferrite production, with an annual output exceeding 300 kilotons, underscoring its commercial and technological significance. Hexaferrites find versatile applications in microwave devices, permanent magnets, computer memory storage, transformers, radio frequency coils, microstrip antennas, magneto-optic devices, and high-density magnetic recording media. Structurally, hexagonal ferrites can be classified into seven types based on their chemical formulas: $MFe_{12}O_{19}$ (M-type), $MB_2Fe_{16}O_{27}$ (W-type), $M_2B_2Fe_{20}O_{46}$ (X-type), $M_2B_2Fe_{12}O_{22}$ (Y-type), $M_3B_2Fe_{24}O_{41}$ (Z-type), $MX_2Fe_4O_{11}$ (R-type), and $M_4B_2Fe_{36}O_{60}$ (U-type), where "M" represents divalent metals such as calcium, strontium, barium, or lead, and "B" typically denotes bivalent transition metal cations including nickel, cobalt, copper, or zinc[7].

Efforts to enhance the electrical and magnetic properties of M-type hexaferrites have involved doping strategies with various cations. Substitution of Fe^{3+} ions with trivalent cations such as Al^{3+}, Ga^{3+}, In^{3+}, Sc^{3+}, Cr^{3+}, and La^{3+}, as well as co-doping with divalent and trivalent ion pairs like Ho^{3+}-Ni^{2+}, Nd^{3+}-Zn^{2+}, La^{3+}-Co^{2+}, and Al^{3+}-Co^{2+}, have been shown to refine their properties. Additionally, replacing base divalent and tetravalent ions with dopants such as Zn^{2+}–Mo^{4+}, Ti^{2+}–Ru^{4+}, Co^{2+}–Sn^{4+}, and Co^{2+}–Ti^{4+} offers further control over magnetic and electrical behavior, tailoring these materials for specific applications. M-type hexaferrites are particularly attractive for high-frequency applications due to their excellent chemical stability, relatively high magnetization, and elevated Curie temperatures. Their high resistivity and low eddy current losses make them superior to many other magnetic materials for use in microwave devices, multilayer resonant circuits, chip inductors, circulators, and magnetic recording media. Key electrical and magnetic properties such as grain size, dielectric permittivity, loss tangent, resistivity, and ac conductivity can be optimized through careful doping, annealing, compositional control, and choice of synthesis technique[8, 9].

Various synthesis methods have been employed for producing M-type hexaferrites, including co-precipitation, ball milling, micro-emulsion, glass ceramic, hydrothermal, wet mixing, and sol-gel processes[10-12]. Among these, the sol-gel method is particularly favored due to its advantages such as shorter reaction times, energy efficiency, lower annealing temperatures, production of ultrafine and uniform nanopowders, simplicity, cost-effectiveness, and the ability to form single-domain particles with controlled size distribution[13-15]. This bottom-up chemical process transforms a homogeneous sol into a dense three-dimensional gel network, facilitating the production of hexaferrites with optimal magnetic coercivity for recording applications. Although extensive research has been conducted on the preparation and characterization of M-type hexaferrites, studies on specific compositions such as $Ca_{1-x}Bi_xFe_{12-x}Co_xO_{19}$ remain limited. Previous investigations have explored magnetic and dielectric properties in various doped hexaferrites, highlighting the influence of compositional and temperature variations on their behavior. Continued research into such materials is essential to further advance their functional properties for emerging technological demands[16].

This research focuses on the synthesis of transition metal-doped vanadium and graphene-based nanostructures using controlled chemical methods and their thorough

Annual Methodological Archive Research Review
http://amresearchreview.com/index.php/Journal/about
Volume 3, Issue 10 (2025)

Online ISSN 3007-3197
Print ISSN 3007-3189

http://amresearchreview.com/index.php/Journal/about

characterization to assess their multifunctional properties. The study aims to examine the optical, structural, morphological, and dielectric properties of the synthesized nanocomposites by employing ultraviolet-visible (UV-Vis) spectroscopy, Fourier transform infrared (FTIR) spectroscopy, powder X-ray diffraction (PXRD), scanning electron microscopy (SEM), and dielectric measurements. Particular emphasis will be placed on determining the band gap energy, identifying functional groups, analyzing crystallinity, evaluating surface morphology, and understanding the dielectric behavior of the materials. The findings of this research are expected to advance the synthesis optimization and demonstrate the potential of these nanostructures for applications in electronics, sensing, energy storage, and environmental technologies.

Materials and Methods

Synthesis of M-type Hexagonal Ferrites

M-type hexagonal ferrites synthesis by the known concentration calcium and chromium nitrate, Iron nitrate, Barium nitrate,) and Citric acid, both are 99.9% pure. Sol-gel auto-combustion was used to create M-type hexaferrites with the following chemical formulas: $Ca_{0.25}\,Ba_{0.75}C_{rx}Fe_{12-x}O_{19}$ with x = (0.0, 0.05, 0.10, 0.15, and 0.20). To create a homogenous solution, these above mentioned metallic nitrates have all been combined with filtered water & stirred. The chelator utilized as citric acid. NH_3 solution was utilized to maintain the mixture neutrality. At 80 °C, a homogeneous mixture was produced. The mixture was continuously heated & stirred until it grew highly viscous and finally took the shape of a brownish gel. Citric acid and metal nitrates were preserved at such a 2:1 ratio. Around 80 °C with continuous stirring or burning, the gel begins to fire out due to the rise in temp. Afterwards, a mortar and pestle were used to grind the frothy powder. In order to achieve the stable state of metal ions and produce M-type hexagonal ferrites form, the finely ground powdered was subsequently annealed at 1200°C for 8hours in a rising temperature-controlled muffle furnace called Vulcan (A.550)]

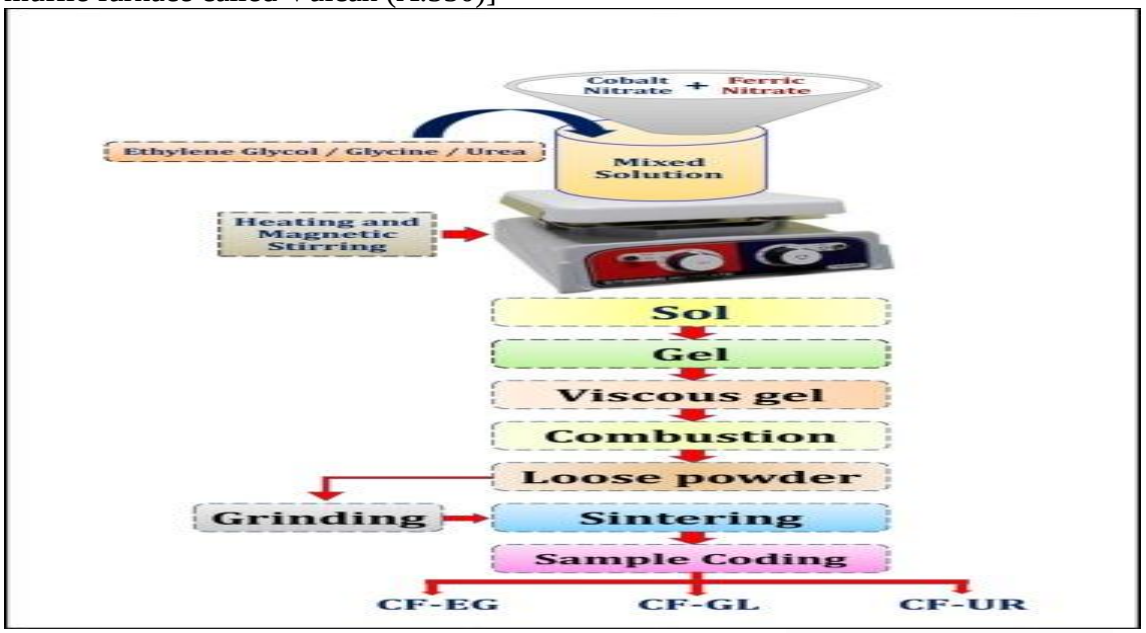


Figure Error! No text of specified style in document..**1.** Sol-gel auto combustion

Annual Methodological Archive Research Review
http://amresearchreview.com/index.php/Journal/about
Volume 3, Issue 10 (2025)

Online ISSN 3007-3197
Print ISSN 3007-3189
http://amresearchreview.com/index.php/Journal/about

method

Experimental Work

Materials: Iron nitrate $Fe(NO_3)_3.9H_2O$, Citric acid, $C_6H_8O_7.H_2O$, Barium nitrate $Ba(NO3)_2$, Chromium nitrate $Cr(NO3)_3$, Calcium nitrate $Ca(NO_3)_2$ and distilled water were employed in this experiment.

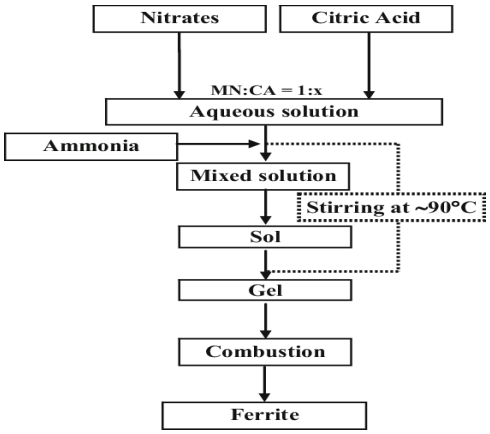


Figure Error! No text of specified style in document..**2.** Flowchart of solgel method

Results and Discussion

UV-Vis Spectroscopy

Band gap energy

Optical analysis of $Ca_{0.25}Ba_{0.75}Cr_xFe_{12-x}O_{19}$ (x = 0, 0.05, 0.10, 0.15, 0.20) was carried out and it showed that the variation in absorbance was based on the band gap, the grain size and the oxygen moieties. [17]. Tauc's plot had been employed in order determine the band gap energies. (Eq.1)

$$a = \frac{(hv - E_g)^{n}/_{2}}{hv} \qquad (1)$$

Where, 'α', 'n', 'Eg', 'h' and 'v' are the absorbance coefficient, nature of transmission, band gap energy, Planck's constant and frequency of incident photon. Undoped barium hexaferrite had a straight band gap of 3.16 eV. The energy of the band gap was reduced from 3.16 (eV) to 2.49 (eV) after rising their doping amount. The inclusion of dopant metal ions resulted in a decrease in band gap energy. The Cr^{+2} as well as Fe^{+2} ions produce energy levels among the VB and the CB. Light particles through the sub-band separation are absorbed by the integrated intermediate states affecting the spectral absorption. The decline in the band gap value may also be related to the reduction in crystallite size. [18]. A decrease in energy band gap demonstrated that the materials might be used in solar cells for photocatalysis to capture energy from the sunlight. [19].

Annual Methodological Archive Research Review
http://amresearchreview.com/index.php/Journal/about
Volume 3, Issue 10 (2025)

Online ISSN 3007-3197
Print ISSN 3007-3189

http://amresearchreview.com/index.php/Journal/about

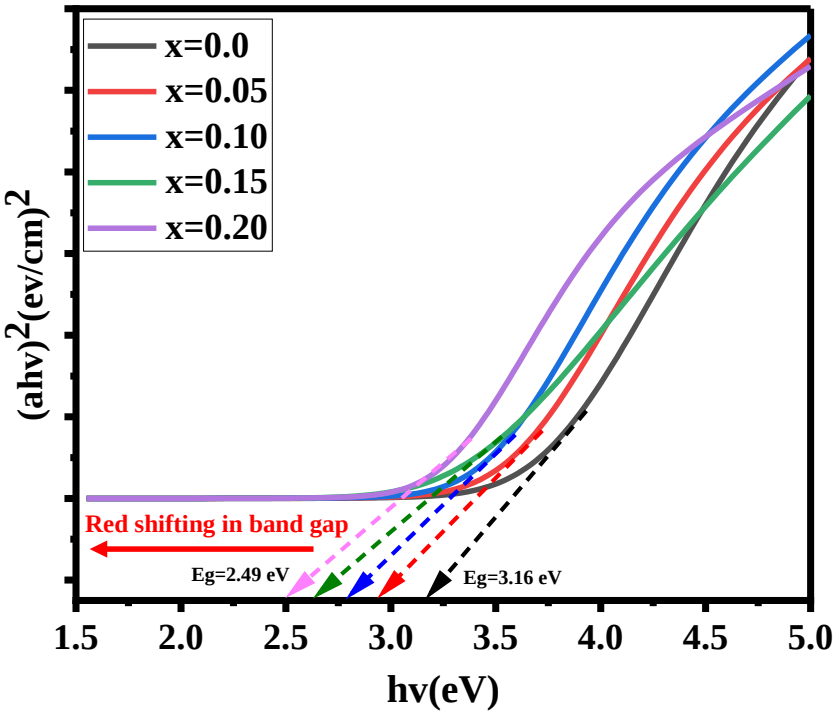


Figure Error! No text of specified style in document..**3:** Tauc Plot of $Ca_{0.25}Ba_{0.75}Cr_xFe_{12-x}O_{19}$ (x = 0, 0.05, 0.10, 0.15, 0.20)

XRD Analysis

The XRD pattern of all composition $Ca_{0.25}Ba_{0.75}Cr_xFe_{12-x}O_{19}$ (x = 0, 0.05, 0.10, 0.15, 0.20) hexaferrite shown in figure 4.1. The samples were annealed at 1200°C for 8h. Figure 4.1 shows the material's excellent crystalline nature that is represented by the peaks sharpness and intensity. The peaks at approximately angle 2theta values are 31.81°, 40.91°, 43.52°, 54.13°, 57.04° were labeled as (112), (205), (1010), (302), (218) planes. With the standard card number reported by the M-type hexaferrites have hexagonal shape with the spatial class P63/mmc, all of the peaks were accurately identified. In the XRD pattern, there are no more peaks or phases. For x=0 The sample represents un substitute chromium material, whereas the patterns of other samples revealed chromium substitution. It must be found that the (110) peak changes gradually towards the greater angle, as a consequence of such crystal lattice shrinking with the replacement of dopant (Cr^{3+}) ions[20].Figure 4.1 represents the $Ca_{0.25}Ba_{0.75}Cr_xFe_{12-x}O_{19}$ hexaferrite Xrd structure.

Annual Methodological Archive Research Review
http://amresearchreview.com/index.php/Journal/about
Volume 3, Issue 10 (2025)

Online ISSN 3007-3197
Print ISSN 3007-3189

http://amresearchreview.com/index.php/Journal/about

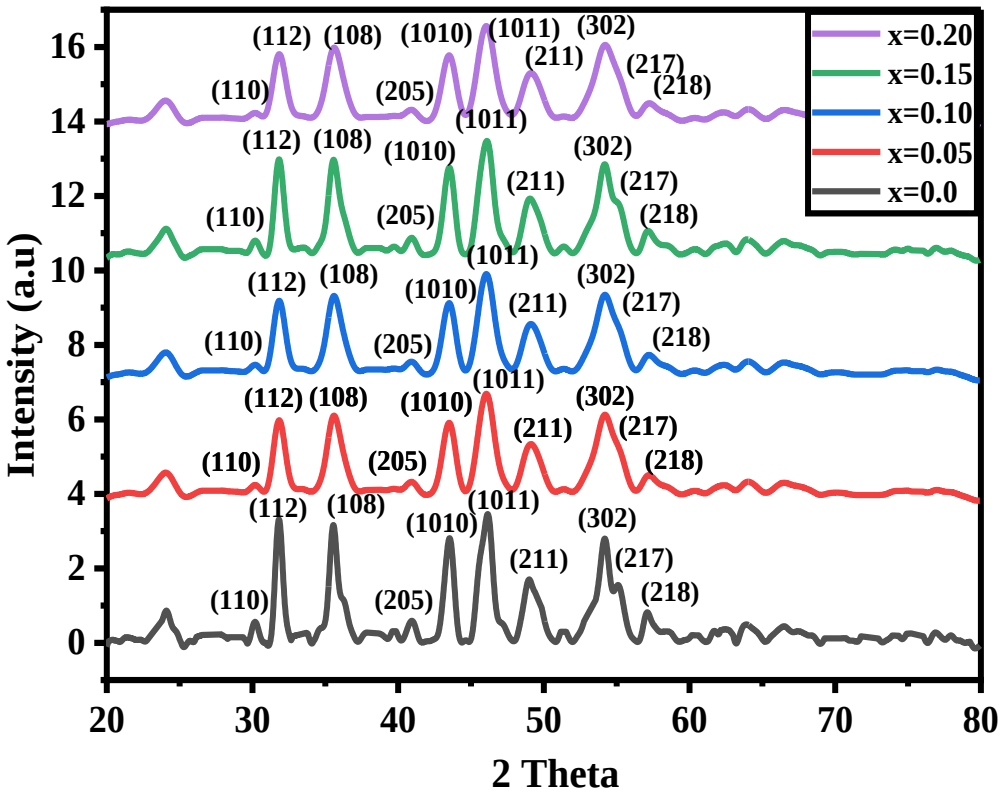


Figure Error! No text of specified style in document..**4.** Combined graph of XRD at $Ca_{0.25}Ba_{0.75}Cr_xFe_{12-x}O_{19}$ (x = 0, 0.05, 0.10, 0.15, 0.20)

Table Error! No text of specified style in document..**1:** XRD values of M-type $Ca_{0.25}Ba_{0.75}Cr_xFe_{12-x}O_{19}$ (x = 0, 0.05, 0.10, 0.15, 0.20)

SR. No.	2theta	theta	FWHM	D(Angstrom)	D(nm)	h k l	Lattice parameter (Å)	Crystal System
1	30.17	15.085	0.18	451.879059	45.18790586	110	5.844	Hexagonal
2	31.81	15.905	0.182	448.690101	44.86901013	112	5.926	Hexagonal
3	35.55	17.775	0.184	448.219513	44.82195126	108	5.925	Hexagonal
4	40.94	20.47	0.187	448.28186	44.82818598	205	5.986	Hexagonal
5	43.53	21.765	0.19	445.072184	44.50721845	1010	6.05	Hexagonal
6	46.46	23.23	0.192	445.125207	44.51252073	1011	6.0878	Hexagonal

Annual Methodological Archive Research Review
http://amresearchreview.com/index.php/Journal/about
Volume 3, Issue 10 (2025)

Online ISSN 3007-3197
Print ISSN 3007-3189
http://amresearchreview.com/index.php/Journal/about

7	48.99	24.495	0.192	449.494045	44.94948573	211	6.135	Hexagonal
8	54.18	27.09	0.192	459.442857	45.94428573	302	6.1822	Hexagonal
9	55.08	27.54	0.192	461.310314	46.13103138	217	6.2294	Hexagonal
10	57.1	28.55	0.192	465.662866	46.56628657	218	6.2766	Hexagonal

Lattice parameters

Table 4.1 shows the variations in the lattice constants, XRD, bulk density, porosity, and phase of $Ca_{0.25}Ba_{0.75}Cr_xFe_{12-2x}O_{19}$ ferrite combinations with Cr concentration (x). Table 4.1 clearly shows that the replacement causes a quick shift in lattice parameters (c) and a gradual fluctuation in lattice parameter (a) . Given that hexagonal ferrites have a constant lattice parameter "a" as well as a variable lattice parameter “c”[21].

Table 4.2 displays the a and c lattice parameters. It was observed that whenever the amount of dopant ion increased, the a and c lattice parameters decreased. Due to some internal lattice distortion brought on by the doping impact of ions with different radii, as well as the ionic radius of chromium is smaller (0.63Å) then iron's (0.64Å), its lattice parameters have decreased[22]. Up to x =0.10 (Cr^{3+}) ions are thought to approach the iron site, then at x > 0.10, greater (Cr^{3+}) ions are thought to be prevented from entering at the iron site, So, part of the chromium ions enter the calcium ion and it may impact the dielectric characteristics of iron-based hexaferrites[23].

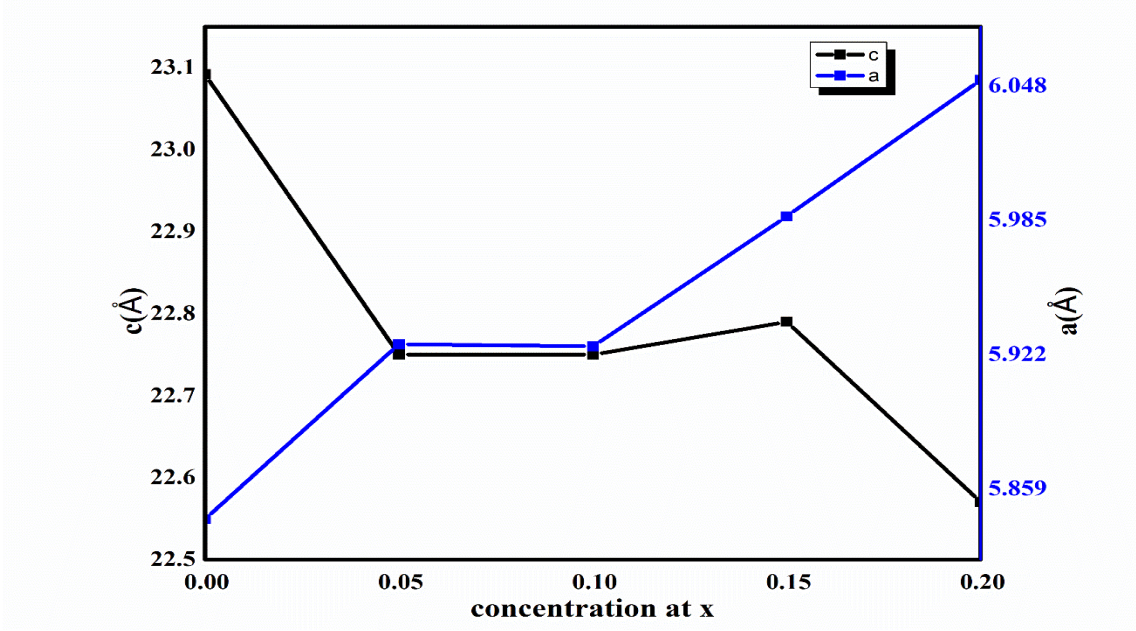


Figure Error! No text of specified style in document..**5.** Lattice constant a and c graph

The fluctuation in lattice constants a and c as a factor of (Cr^{3+}) concentration is shown in Figure 4.2. The graph clearly indicates that when c declines tremendously, the amount almost stays unchanged. This fact that 'a' in hexaferrites is a smaller lattice

Annual Methodological Archive Research Review
http://amresearchreview.com/index.php/Journal/about
Volume 3, Issue 10 (2025)

Online ISSN 3007-3197
Print ISSN 3007-3189

http://amresearchreview.com/index.php/Journal/about

parameter than 'c'. However, due to the discrepancy in ionic radii between the base and dopant elements, c decrease significantly.

The fluctuation in the c/a ratio and cell volume(V) is seen in Figure 4.3. Cell volume(V) decreases monotonically when the doped c/a ratio rises. This is caused by the constant value of "a" as the amount of dopant element increases. Table 1 shows that the c/a ratio ranges between 3.9514 to 3.7305. This type of structure can also be identified by using the c/a ratio. It might be lower or equivalent to 3.98 for a hexagonal structure. The M-type hexagonal ferrite structure is proved if the c/a value is smaller than 3.980, say Yujie Yang and Duohui Huang.[24].

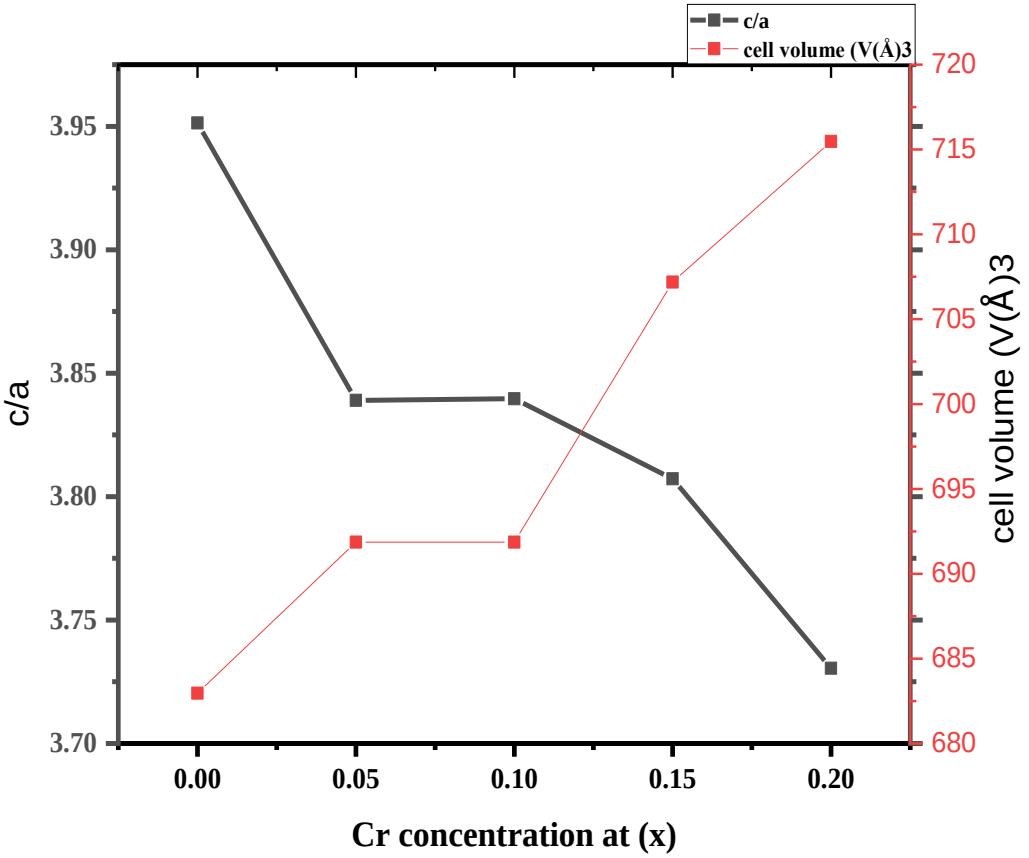


Figure Error! No text of specified style in document.**.6.** Graph between cell volume V(Å)^3 and c/a

The following is a chart that compares structural characteristics with earlier research on iron-based M-type hexaferrites. It is seen from the table that our findings on lattice parameters a, c, cell volume(V), and crystallite size(D) are consistent with earlier research[25, 26].

Annual Methodological Archive Research Review
http://amresearchreview.com/index.php/Journal/about
Volume 3, Issue 10 (2025)

Online ISSN 3007-3197
Print ISSN 3007-3189

http://amresearchreview.com/index.php/Journal/about

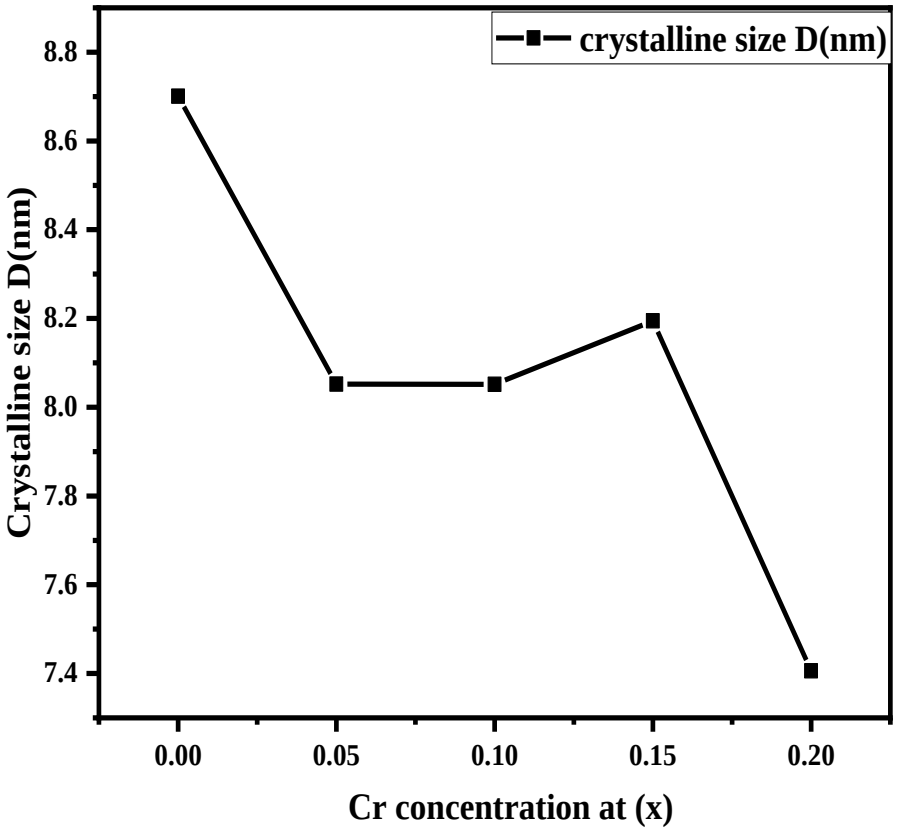


Figure Error! No text of specified style in document..**7.** Graph of crystalline size

Table 4.2 also makes clear that when the Cr concentration(x) increases, the bulk density (m) also rises. Furthermore, it has been shown that bulk density values are significantly lower than X-ray density values. Its smaller value (P_m‹P_x) is explained by the pore formation processes that take place during synthesizing. Volume loss can be attributable to the rise in bulk density.

it can be seen that the porosity (%P) and X-ray density (P_x) both decreases due to the the increasing doping of chromium content (x) in $Ca_{0.25}Ba_{0.75}Cr_xFe_{12-2x}O_{19}$. Higher molar masses of substituted samples are responsible for the drop in X-ray density that results from the substitution of Cr.

With a rise in Cr concentration(x), the porosity(P) of all of the specimens under consideration falls. The fall in X-ray density are responsible due to the decrease in porosity. The aggregation of particles during combustion synthesis may be the cause of the high porosity values.

Annual Methodological Archive Research Review
http://amresearchreview.com/index.php/Journal/about
Volume 3, Issue 10 (2025)

Online ISSN 3007-3197
Print ISSN 3007-3189

http://amresearchreview.com/index.php/Journal/about

Lattice parameters

Table Error! No text of specified style in document.**.2:** Lattic parameters a and c of $Ca_{0.25}Ba_{0.75}Cr_xFe_{12-x}O_{19}$ (x = 0, 0.05, 0.10, 0.15, 0.20)

content	a(Å)	c(Å)	c/a	Cell volume $V(Å)^3$	D(nm)	P_x (g/cm-3)	P_b (g/cm-3)	%Porosity (P)%
0.0	5.854	23.082	3.9514	681.96	8.701	5.299	3.351	36
0.05	5.926	22.75	3.839	691.866	8.052	5.194	3.545	32
0.10	5.925	22.751	3.8496	691.876	8.056	5.227	3.645	32
0.15	5.986	22.790	3.8072	707.1896	8.1946	5.10	3.443	32
0.20	6.050	22.570	3.7305	715.48	7.4058	5.04	3.64	27

Dielectric Properties

Dielectric constant

Ferrites' dielectric behaviour represents one of its important properties. For example the synthesis techniques, heat, and sintered duration, dielectric characteristics may be tailored characteristics. In the frequency between 1 MHz to 3 GHz, the dielectric characteristics of $Ca_{0.5}Ba_{0.75}Cr_xFe_{12-x}O_{19}$ (x = 0.0, 0.05, 0.10, 0.15, and 0.20) hexaferrites were examined[27].The equation(4.8) may be used to compute dielectric constant.

$$\acute{\varepsilon} = Cd/A\varepsilon_{\circ} \qquad (4.8)$$

wherein C would be the capacitance, d seems to be the pellets thickness, ″A″ represents the cross-sectional surface, while "$\varepsilon_{\circ}$" is the permittivity of blank space[28]. According to Figure 4.5, hexagonal ferrites often exhibit a reduction in dielectric permittivity when rises in frequency. This happens as a result of interfacial polarization predicated that Koops theory and Maxwell-Wagner concept, in addition to hopping across Fe^{+3} or Fe^{+2} as well as conducting layers inside the substrate. Since hexagonal ferrite grains were efficient at low frequency whereas grain boundaries become efficient at higher frequency, the dielectric permittivity is greater at low frequency range[29].The vibrating intensity is less at higher frequency. Moving electrons can go to grain boundary as a result of the hopping phenomenon, and this causes polarization to occur. The increased vibrating amplitude at lower frequency is due to something like this[30]. This is brought on by an induced external electric field. Greater domain results in a fixed value because the polarization of the produced electric field could not resonant as frequency rises[31].

Annual Methodological Archive Research Review
http://amresearchreview.com/index.php/Journal/about
Volume 3, Issue 10 (2025)

Online ISSN 3007-3197
Print ISSN 3007-3189

http://amresearchreview.com/index.php/Journal/about

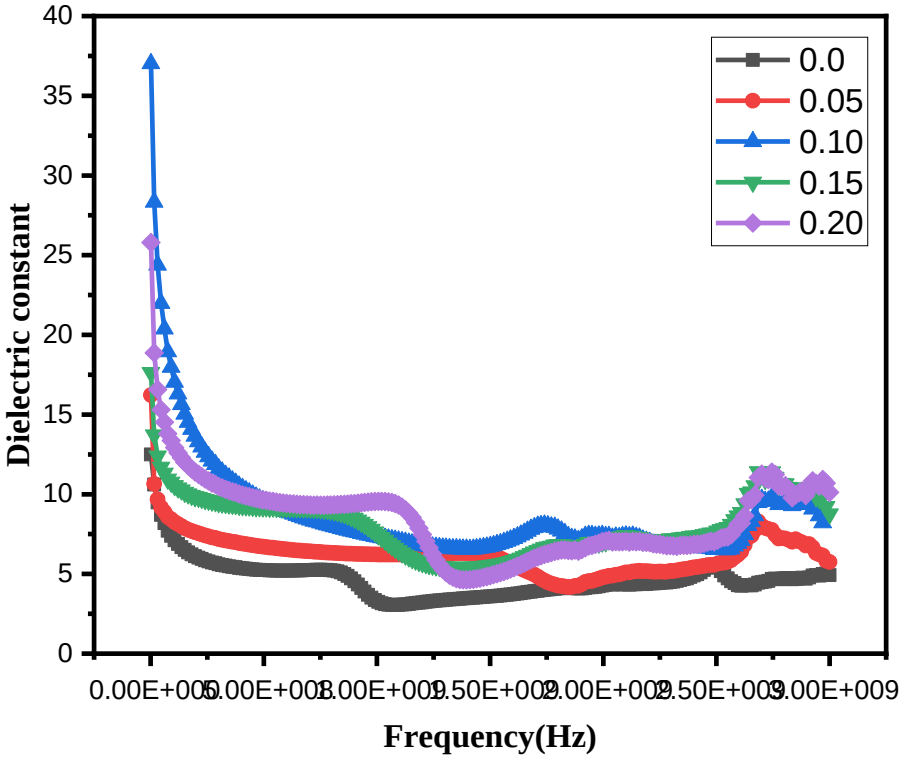


Figure Error! No text of specified style in document.**.8.** $Ca_{0.5}Ba_{0.75}Cr_xFe_{12-x}O_{19}$ (x =0.0,0.05,0.10,0.15, and 0.20) M-type hexaferrites dielectric constant variations vs frequency.

Dielectric loss

Here, in Equation(4.5), is the expression representing dielectric loss.

$$\varepsilon'' = \acute{\varepsilon} \tan \delta \qquad (4.5)$$

Here tanδ is the tangent loss, έ is the relative permittivity, and ε″ is the dielectric loss element Fig.6 displays the maxima of the dielectric loss values. As rise in frequency, the dielectric loss reduces. Such a loss caused by the eddy current losses in ferrites at greater frequencies even though greater frequencies cause lattice distortion, which increases resistivity. At lower frequencies, the dielectric loss was initially high and by further substitution it gradually decreased and became constant, but as frequency increased, the dielectric loss decreased. Low dielectric loss in rising domain indicated that greater energy loss is reduced. A resonant spike is observed at the frequency of 2.1GHz as a result of the inherent dipole moment or interfacial polarization. When the external applied field reaches the hopping frequency, the losses is at its greatest. Up to x = 0.10 dielectric loss losses is observed to rise. However, when the Chromium(Cr^{3+}) content is substituted more, dielectric loss is shown to reduce.

Annual Methodological Archive Research Review
http://amresearchreview.com/index.php/Journal/about
Volume 3, Issue 10 (2025)

Online ISSN 3007-3197
Print ISSN 3007-3189

http://amresearchreview.com/index.php/Journal/about

$Ca_{0.25}Ba_{0.75}Cr_xFe_{12-x}O_{19}$ has the lowest dielectric loss at GHz frequency range between all synthesized materials. It could be caused by cations occupying multiple crystallographic positions with in Calcium M-type hexaferrites, as well as by disruption of the grains and grain boundaries[32].

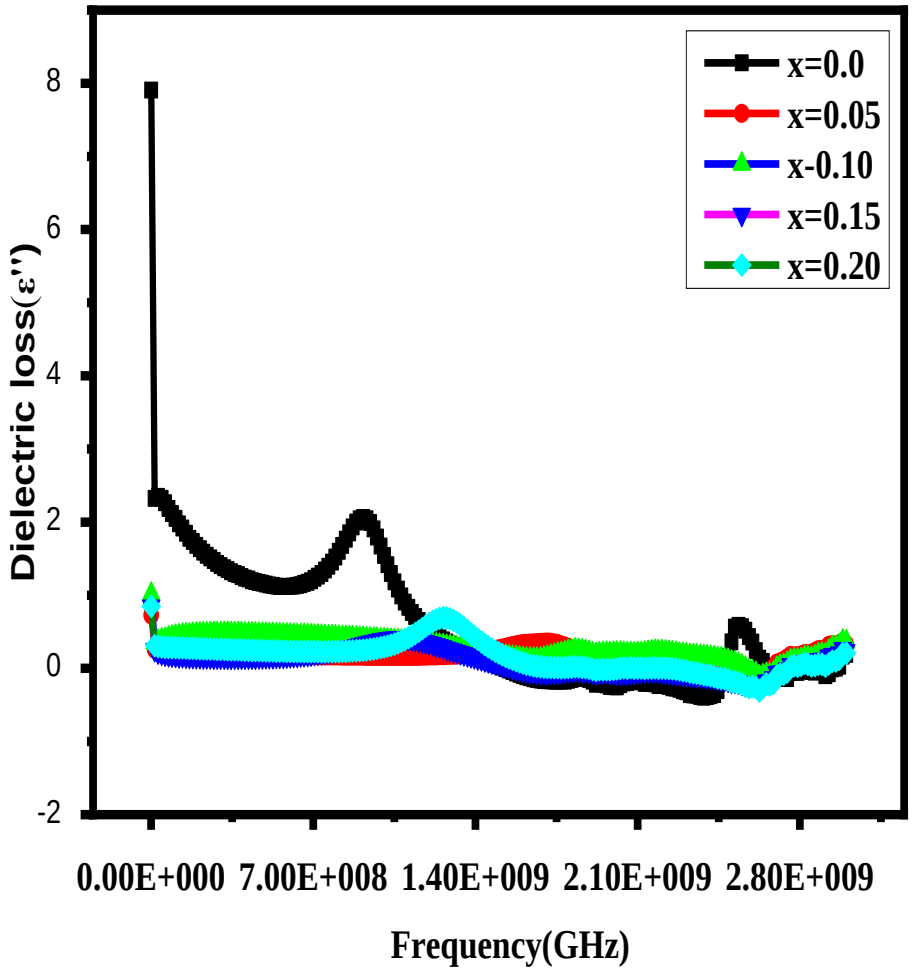


Figure Error! No text of specified style in document..**9.** Change of the dielectric loss of $Ca_{0.25}Ba_{0.75}Cr_xFe_{12-x}O_{19}$ M-type hexaferries vs frequency.

Tan loss

According to Equation(4.6) it is the proportion of the dielectric loss to the dielectric constant[33].

$$\text{Tan } \delta = \varepsilon''/\acute{\varepsilon} \qquad (4.6)$$

displays showing frequency vs the dielectric tangent loss.

Annual Methodological Archive Research Review
http://amresearchreview.com/index.php/Journal/about
Volume 3, Issue 10 (2025)

Online ISSN 3007-3197
Print ISSN 3007-3189

http://amresearchreview.com/index.php/Journal/about

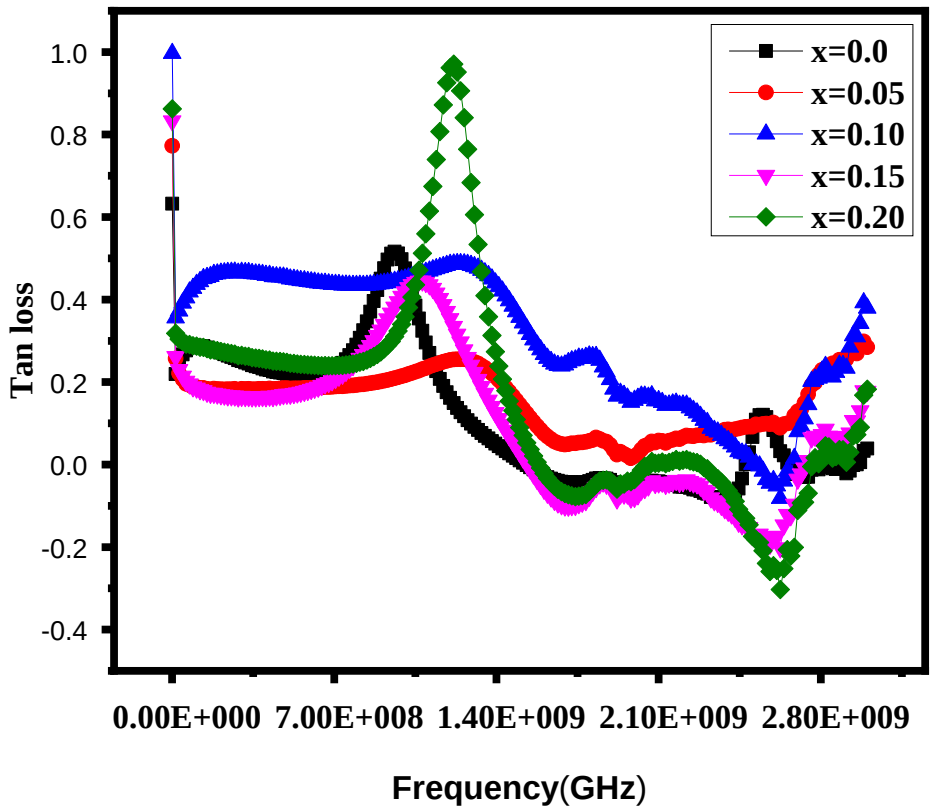


Figure Error! No text of specified style in document..**10.** Modulation of frequency-dependent dielectric tan loss in $Ca_{0.5}Ba_{0.75}Cr_xFe_{12-x}O_{19}$ M-type hexaferrites

Tangent loss is significant at low frequency and diminishes as frequency increases. Around 2 GHz, a resonant waveform is seen when the hopping frequencies approaches the outside applied electric field frequency. This resonance phenomenon is also caused by P- or N-type charges carriers[34]. The replacement of Cr results in a reduce in tan losses at greater frequencies, which then in turn lowers energy losses. Dielectric tan loss makes for a sizable amount of the total core loss in ferrites. Dielectric loss are mildly induced by a little core loss. when the Chromium(Cr^{3+}) concentration rises, the dielectric tan loss rises at lower frequencies while dropping near about ε″ at greater frequencies.

A.C conductivity

The ac conductivity is determined using equation (4.7).

$$\sigma'_{ac} = \omega\varepsilon_0\acute{\varepsilon}\tan\delta \qquad (4.7)$$

we know that, $\omega = 2\pi f$

Figures (4.8) depicts that the curve of normal temperature ac conductivity as just a function of frequency. The information in Fig(4.8) that frequency-dependent ac conductivity rises.[35] This would be owing to the fact that conductance improves at

Annual Methodological Archive Research Review
http://amresearchreview.com/index.php/Journal/about
Volume 3, Issue 10 (2025)

Online ISSN 3007-3197
Print ISSN 3007-3189

http://amresearchreview.com/index.php/Journal/about

greater frequencies because of the electrons hopping, which is decreased at shorter frequencies when iron(Fe^{+2}) and iron(Fe^{+3}) are present[36].Based on the Maxwell Wagner & Koop model, ferrites are made up of conductive particles that are separated from one another by such a light coating of grain boundary. Both ac conductivity or grain conductivity with greater frequencies are explained by a grain boundaries at lower frequencies. The orientation of grains or grain boundary is arbitrary at low frequency range, however as frequency increases, it become much more orderedly arranged, improving conductivity at greater frequencies. Ac conductivity rises at Cr^{3+} doped up to x = 0.10 and thereafter marginally declines with such a rise in dopant concentration.

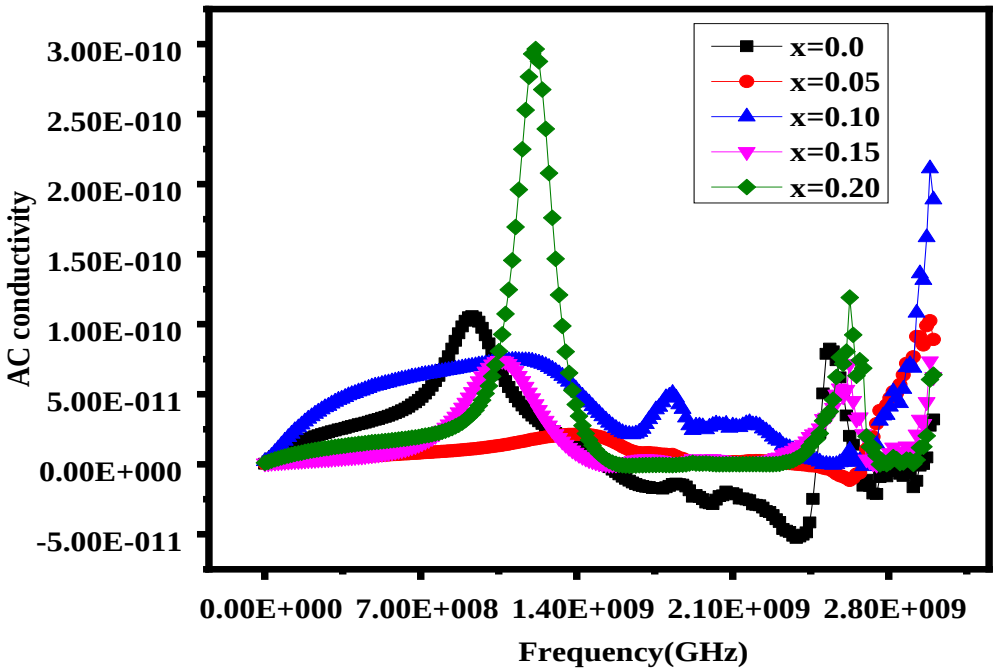


Figure Error! No text of specified style in document..**11.** $Ca_{0.25}Ba_{0.75}CrxFe_{12-x}O_{19}$ M-kind of Hexaferrites ac conductivity verses frequency fluctuations are shown in Fig.4.4 (x = 0 0.05 0.10, 0.15, 0.20)

Q-value

The Q value, which is expressed by the equation Eq(4.8) constitutes the most significant dielectric characteristics. (4.8) as said here:

$$Q=1/\tan\delta \qquad (4.8)$$

Annual Methodological Archive Research Review
http://amresearchreview.com/index.php/Journal/about
Volume 3, Issue 10 (2025)

Online ISSN 3007-3197
Print ISSN 3007-3189

http://amresearchreview.com/index.php/Journal/about

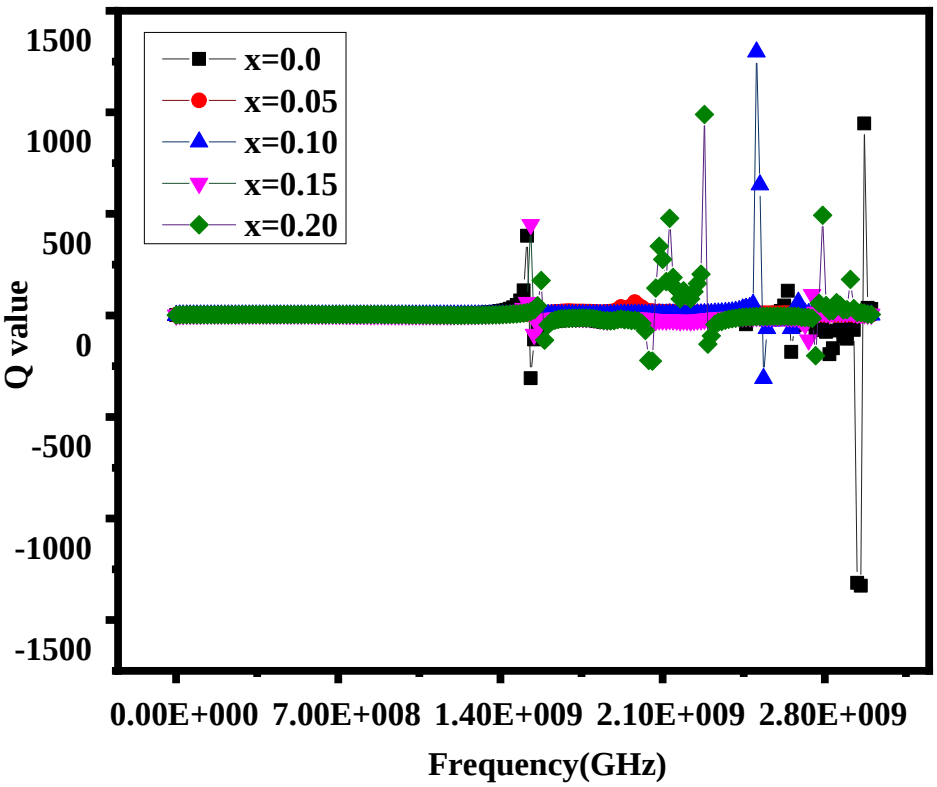


Figure Error! No text of specified style in document..**12.** $Ca_{0.25}Ba_{0.75}Cr_xFe_{12-x}O_{19}$(x = 0 0.05 0.10, 0.15, 0.20) M-kind of Hexaferrites Q-value verses frequency fluctuations are shown in Figure.4.9.

It will seen in Figure 4.5 that perhaps the ratio of Q-value versus frequency rises as doped ion concentration rises. The decrease in loss between (1.2 to 2.3 GHz) results produce a high result when x = 0. It has been demonstrated that resonant peaks trend towards a greater frequencies range when doped concentrations rise. Several negatives spikes may be seen in the quality factor Q-value plot[22]. because the processed specimens include holes. Max quality factor Q-value (1305) for specimen when x = 0.10, $Ca_{0.25}Ba_{0.75}Cr_xFe_{12-x}O_{19}$ and at approximately 1.8 GHz frequencies, were noted. Given that perhaps the resonance maxima happened above 1.5 GHz, it is obvious that if these compounds are very well suited to be used in rising frequencies uses and also in parts including frequencies filtration or resonant circuits.

Electric modulus

Formula describes the orignal and fictitious components of the electric modulus. correspondingly (4.9) or (4.10). Electrical modulus is indeed a crucial tool for examining the generated pattern's more salient characteristics, including quiet time, electronic transport characteristics, and hopping rates ions concentration. When the frequencies of circulating dipoles seems to be in phase with resonant frequencies, the

Annual Methodological Archive Research Review
http://amresearchreview.com/index.php/Journal/about
Volume 3, Issue 10 (2025)

Online ISSN 3007-3197
Print ISSN 3007-3189

http://amresearchreview.com/index.php/Journal/about

M′ number reaches the maximum values and becomes consistent across all sampling. Its M′ number is less in the lower frequencies domain or grows with frequencies.[37]. Frequency vs real and unreal parts of the elasticity of the produced $Ca_{0.25}Ba_{0.75}Cr_xFe_{12-x}O_{19}$ (x = 0 0.05 0.10, 0.15, 0.20) M-type hexaferrites are depicted in Pictures 4.11 or 4,12. Such graphs present a wealth of information regarding the occurrence of charge transfer, which further covers the phenomena of electrical transfer, ionic mobility, or conductance Relaxing against speed[38]. Power losses is represented by an unreal component of electrical modulus[39]. Whereas the frequencies area above charge carriers is restricted to something like a potential well made up of short-distance mobility, its frequency area below the greatest peak depict the limitations of electric charge over a vast area. The systems allow plot shows the conductivity relaxing. That highest frequency requirement of electrical modulus is provided in Equation. as stated in (4.11)

$$2\pi f_{max}\tau=1 \qquad (4.11)$$

Here τ is indeed the soothing period connected to probability hopping.

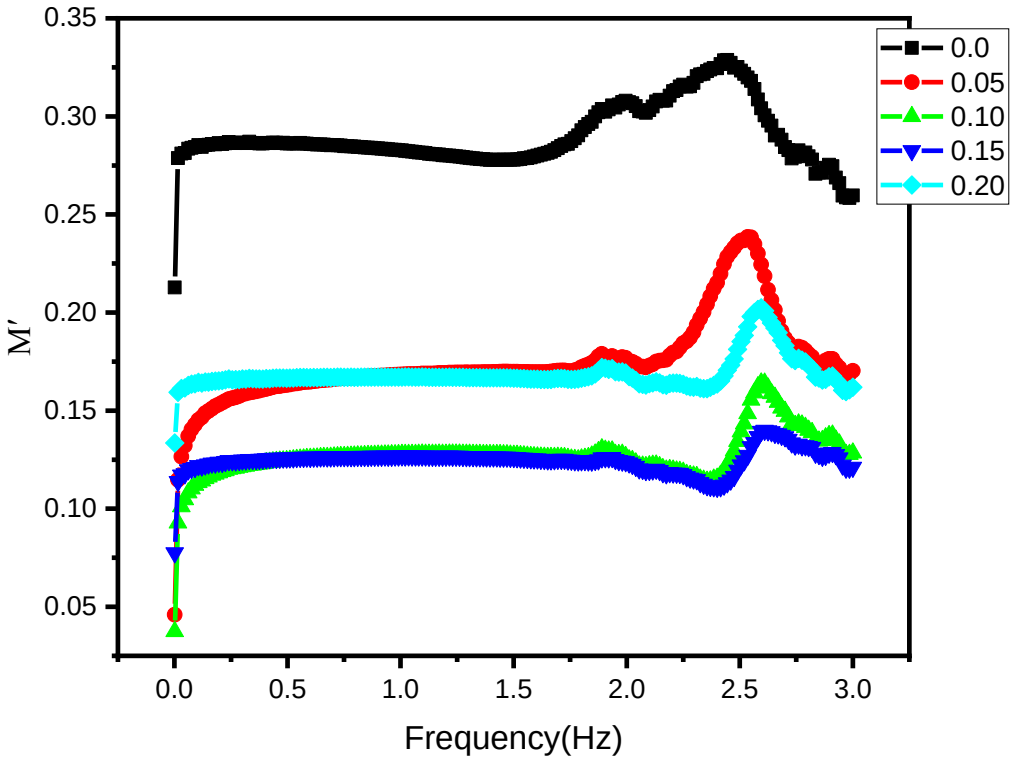


Figure Error! No text of specified style in document..**13.** $Ca_{0.25}Ba_{0.75}Cr_xFe_{12-x}O_{19}$ elasticity varies as frequencies (x = 0 0.5 0.10, 0.15, 0.20) Hexaferrites of group M′.

Annual Methodological Archive Research Review
http://amresearchreview.com/index.php/Journal/about
Volume 3, Issue 10 (2025)

Online ISSN 3007-3197
Print ISSN 3007-3189

http://amresearchreview.com/index.php/Journal/about

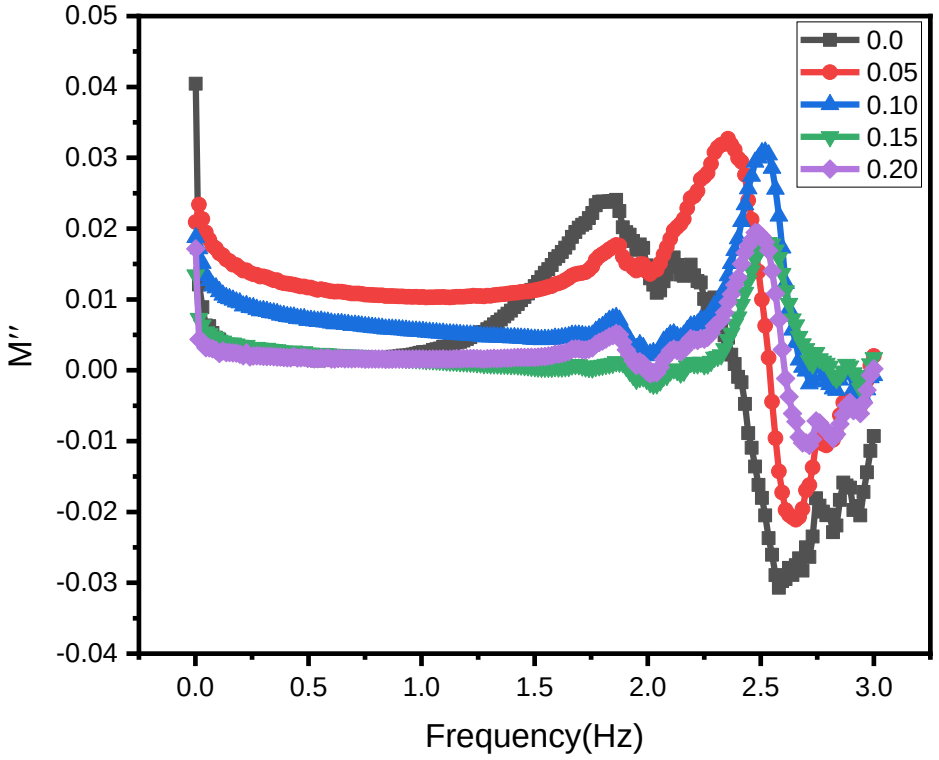


Figure Error! No text of specified style in document..**14.** $Ca_{0.25}Ba_{0.75}Cr_xFe_{12-x}O_{19}$ elasticity varies as frequencies (x = 0 0.5 0.10, 0.15, 0.20) Hexaferrites of group M″.

Scanning Electron Microscopy (SEM)

All sintered hexaferrite samples' SEM micrographs (m) are shown in Figure. S1, S2, S3, S4 and S5. The majority of the grains in the replaced samples are dispersed unevenly throughout the surface and come in a variety of sizes and forms. In samples with x = 0.0, 0.10, and 0.20, the hexagonal platelet-like structure can be seen. All of the substituted samples' grain sizes turn out to be larger than the average crystallite size predicted by the Debye-Scherrer equation (4.4). It is bring about by the aggregation of crystallites, which result from the dipolar attractive contact between magnetic particles [40]. SEM pictures show the average grain size, whereas the average crystallite size shows the average structural coherence length. The mean crystallite size is not equal to the mean physical grain size when the grains are made up of polycrystalline particles; equality only occurs when a single crystal is present. At x = 0.10, a significant number of grain boundaries as well as some grains with a platelet-like structure have developed. As a result of the obstruction to the applied field, coercivity increases when x = 0.10[41]. The SEM pattern of all the samples show that the particles have a well-defined hexagonal form. Scanning electron microscopy (SEM) was used to investigate the shape and particle distribution of

Annual Methodological Archive Research Review
http://amresearchreview.com/index.php/Journal/about
Volume 3, Issue 10 (2025)

Online ISSN 3007-3197
Print ISSN 3007-3189

http://amresearchreview.com/index.php/Journal/about

particles. Figures depict Scanning Electron Microscopy images of lead hexaferrites with Cr^{3+} substitutions. The uniform and regular distribution of grains was seen in figures. However, the particle's size is not constant. The fact that the particle size is bigger than what was predicted by the X-ray diffraction analysis study is caused by the presence of many crystallites inside a single particle. Hexaferrites that have been replaced with Cr^{3+} also exhibit a platelet-like structure.

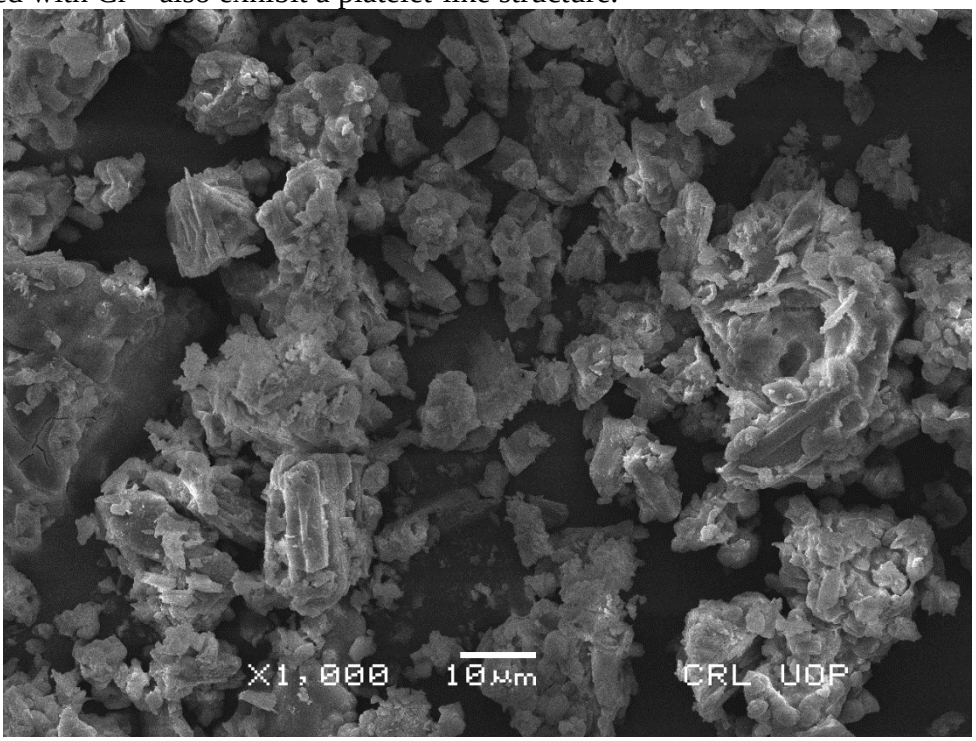
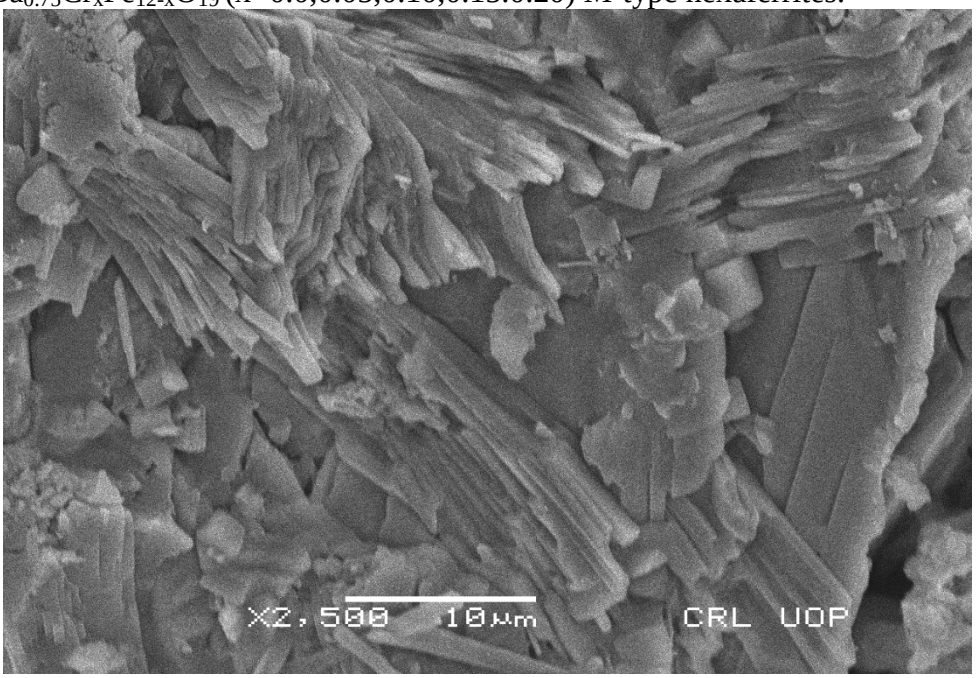


Figure Error! No text of specified style in document.**15.** (S_1) SEM morphology $Ca_{0.25}Ba_{0.75}Cr_xFe_{12-x}O_{19}$ (x=0.0,0.05,0.10,0.15.0.20) M-type hexaferrites.



Annual Methodological Archive Research Review
http://amresearchreview.com/index.php/Journal/about
Volume 3, Issue 10 (2025)

Online ISSN 3007-3197
Print ISSN 3007-3189

http://amresearchreview.com/index.php/Journal/about

Figure Error! No text of specified style in document..**16.** (S_2) SEM morphology $Ca_{0.25}Ba_{0.75}Cr_xFe_{12-x}O_{19}$ at(x=0.0,0.05,0.10,0.15.0.20) M-type hexaferrites.

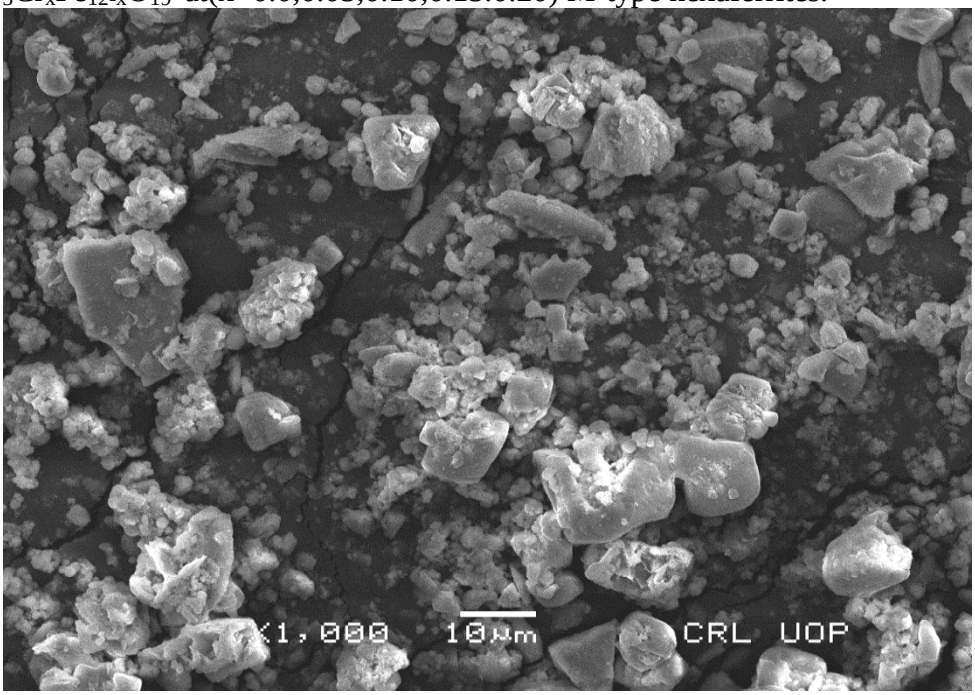


Figure Error! No text of specified style in document..**17.** (S_3) SEM morphology $Ca_{0.25}Ba_{0.75}Cr_xFe_{12-x}O_{19}$ at (x=0.0,0.05,0.10,0.15.0.20) M-type hexaferrites

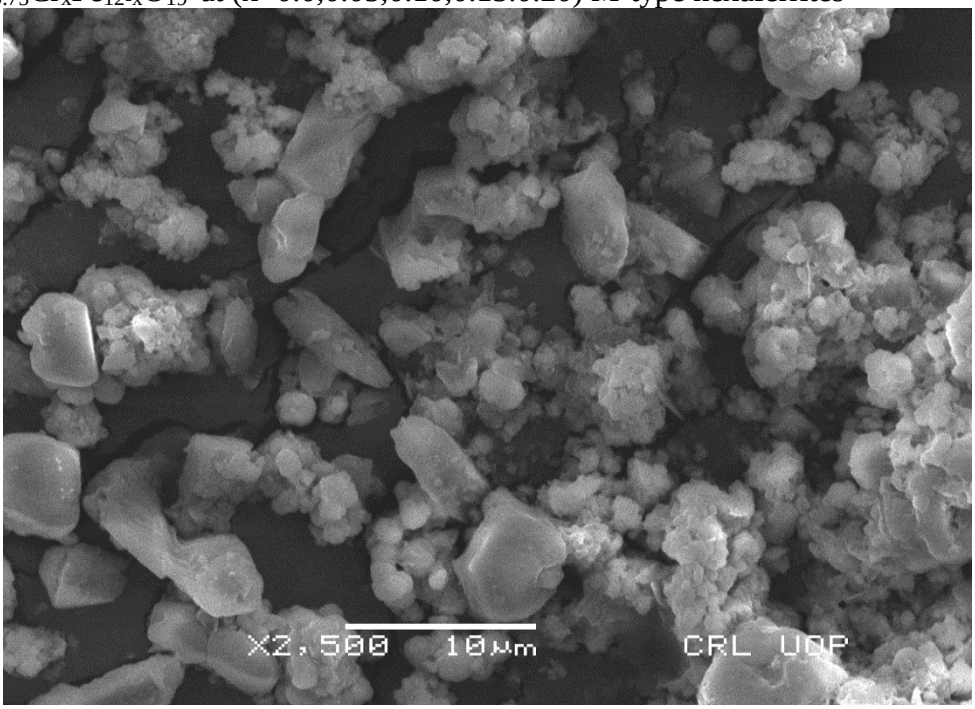


Figure Error! No text of specified style in document..**18.** (S_4) FESEM morphology $Ca_{0.25}Ba_{0.75}Cr_xFe_{12-x}O_{19}$ at (x=0.0,0.05,0.10,0.15.0.20) M-type hexaferrites

Annual Methodological Archive Research Review
http://amresearchreview.com/index.php/Journal/about
Volume 3, Issue 10 (2025)

Online ISSN 3007-3197
Print ISSN 3007-3189

http://amresearchreview.com/index.php/Journal/about

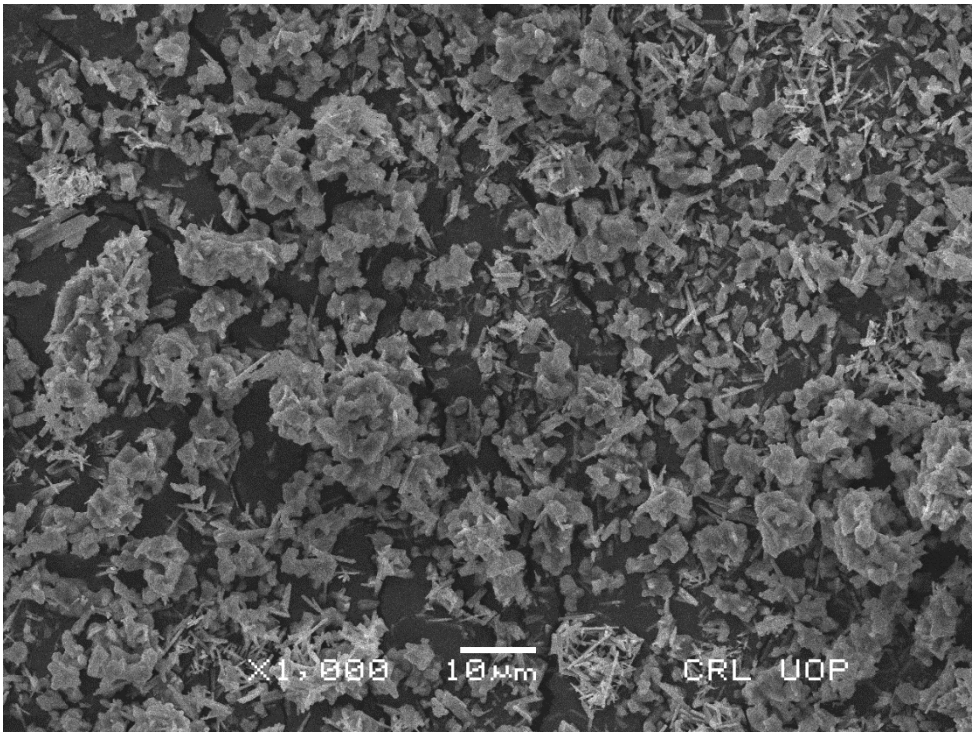


Figure Error! No text of specified style in document.**19.** (S_5) SEM morphology $Ca_{0.25}Ba_{0.75}Cr_xFe_{12-x}O_{19}$ at (x=0.0,0.05,0.10,0.15.0.20) M-type hexaferrites

Conclusion

By using the sol-gel auto-combustion technique, M-type hexaferrites with the formula $Ca_{0.25}Ba_{0.75}Cr_xFe_{12-x}O_{19}$ at (x=0.0,0.05,0.10,0.15.0.20) were successfully created. Optical band gap ranging from 3.16 eV to 2.49 eV having red shift. The primary phase development of the hexagonal platelet shape with P63/mmc group is shown by the XRD pattern of the synthesized samples. . These lattice parameter between a = (5.844-6.050)A˚ c = (23.092-22.570)A˚. The development of the hexagonal phase and the uniform dispersion of the grains are confirmed by SEM data. According to the Maxwell-Wagner and Koop's Model, the dielectric constant, dielectric loss, and tangent loss all show a decreasing tendency. Ferrites ac conductivity is significantly influenced by the hopping phenomena between Fe^{+3} and Fe^{+2}. When Calcium-Barium hexaferrites are substituted with Cr^{3+},dielectric loss and tangent loss are decreased.For sample $Ca_{0.25}Ba_{0.75}Cr_xFe_{12-x}O_{19}$, the Q-value and ac conductivity are determined to be at their maximum value at 1350. Overall summary, such compounds are advised for use in high-frequency applications like electronic gadgets, sensors, submersible pumps, power switches, microwave devices, and longitudinal storage media because of the reduction in dielectric constant and dielectric losses caused by the addition of Cr^{+3}.

Refrence

Zahid, M., et al., Influence of Cobalt on Structural, Morphological, Dielectric, and Magnetic Properties of Barium M-Type Hexagonal Ferrites for Technological Applications. Brazilian Journal of Physics, 2025. **55**(2): p. 62.

Online ISSN 3007-3197
Print ISSN 3007-3189
http://amresearchreview.com/index.php/Journal/about

Kaur, P., S.B. Narang, and S. Bahel, Physical and magnetic properties of Mn–Zr doped La–Sr ferrite prepared by the auto-combustion route. Ceramics International, 2016. **42**(8): p. 9830-9835.

Naqvi, S.T.A., et al., Investigation of structural, hysteresis, and microwave dielectric/magnetic properties of Co-Zn doped M-type strontium hexaferrites for light-weight microwave absorber applications. Emergent Materials, 2025: p. 1-23.

Singh, C., et al., Temperature and frequency tuned study of electrical properties of M-type strontium hexaferrite. Ceramics International, 2025. **51**(9): p. 11593-11602.

Zubair, B., et al., Tailoring Properties of Co-Sm Substituted Ba-Ni W-type Hexagonal Ferrites for Next-Generation Electronics and Antibacterial Materials. Ceramics International, 2025.

Kalia, S., R. Jasrotia, and V.P. Singh, Magnetic Nanoferrites and Their Composites: Environmental and Biomedical Applications. 2023: Elsevier.

Dhingra, A., O. Thakur, and R. Pandey, Dielectric Investigations of Al–doped M–type Strontium Hexaferrite. Recent Advances in Functional Materials, Volume 1: Select Proceedings of RAFM 2024, 2025. **1**: p. 237.

Costa, B.F., et al., Mössbauer and Optical Investigations on Sr Doped M-Type BaFe12O19 Hexaferrites Produced via Autocombustion. Crystals, 2025. **15**(4): p. 291.

Himanshi, et al., Sol-gel fabricated barium M-type hexaferrites: Effect of high cobalt doping on the structural, optical, surface, and magnetic traits of BaFe12O19 hexaferrites. Journal of Sol-Gel Science and Technology, 2025: p. 1-13.

Alsharif, M.A., et al., Phase transformation of hexagonal to mixed spinel crystal structure and magnetic properties of Co2+ ions substituted PbFeO. Journal of Sol-Gel Science and Technology, 2025: p. 1-13.

Kumari, P., et al., Exploring effect of lanthanum substitution on physical and magneto-ferroelectric behavior of strontium hexaferrite nanomaterials for its applications in data storage to electronics industries. Journal of Sol-Gel Science and Technology, 2025. **114**(3): p. 1011-1028.

Abbas, M.A., Advanced Synthesis and Multifunctional Characterization of Neodymium-Doped $Ba_2NiCoFe_{28-x}O_{46}$ X-Type Hexagonal Ferrites: A Comprehensive Study of Structural, Morphological, and Electromagnetic Properties. Sch Acad J Biosci, 2025. **8**: p. 1213-1227.

Jasrotia, R., et al., Sol–gel synthesized Mg–Ag–Mn nanoferrites for power applications. Journal of Sol-Gel Science and Technology, 2021. **97**(1): p. 205-212.

Therese, A.M., et al., The effect of different temperature rate on sol-gel approach derived M-type hexagonal BaFe12O19 using D-mannose as a fuel: synthesis, structural, thermal gravimetric and magnetic properties. Journal of the Indian Chemical Society, 2024. **101**(9): p. 101215.

Jagtap, P. and M. Laad, Strontium hexaferrite (SrFe12O19) for smart sensing: a review on synthesis strategies and functional applications. Discover Materials, 2025. **5**(1): p. 184.

Safdar, A., et al., Multifaceted Analysis of Cd-Substituted Ba (Cu2) 2Fe4-xCdxO11

Online ISSN 3007-3197
Print ISSN 3007-3189
http://amresearchreview.com/index.php/Journal/about

R-Type Hexaferrites for Enhanced Data Storage and High-Frequency Applications. Materials Chemistry and Physics, 2025: p. 131426.

Bibi, I., et al., Effect of doping on dielectric and optical properties of barium hexaferrite: Photocatalytic performance under solar light irradiation. Ceramics International, 2021. **47**(22): p. 31518-31526.

Pattanayak, R., et al., Electric transport properties study of bulk BaFe12O19 by complex impedance spectroscopy. Physica B: Condensed Matter, 2015. **474**: p. 57-63.

Khaliq, N., et al., Zn and Mn doped Ba1-xZnxFe12-yMnyO19 as highly photoactive under visible light with enhanced electrochemical and dielectric properties. Materials Science in Semiconductor Processing, 2022. **139**: p. 106324.

Yang, Y., et al., Investigating the influence of Cr-Zn substitution on magnetic and structural properties of M-type SrBaSm hexaferrites Sr0. 6Ba0. 1Sm0. 3Fe12. 0-x (Cr0. 6Zn0. 4) xO19. 2018. **56**(1): p. 67-74.

Kojima, H., Ferromagnetic Materials vol 3, ed EP Wohlfarth. 1982, Amsterdam: North-Holland) p.

Khan, M.A., et al., Structural, spectral, dielectric and magnetic properties of Sr2CuxNi2-xFe28-xCrxO46 (0≤ x≥ 0.5) ferrites synthesized via micro-emulsion route. 2021. **259**: p. 124066.

Kumar, S., et al., Lattice strain mediated dielectric and magnetic properties in La doped barium hexaferrite. 2019. **473**: p. 312-319.

Yang, Y., et al., An investigation on microstructural, spectral and magnetic properties of Pr–Cu double-substituted M-type Ba–Sr hexaferrites. 2019. **57**: p. 250-260.

Yang, Y., et al., Influence of Nd-NbZn co-substitution on structural, spectral and magnetic properties of M-type calcium-strontium hexaferrites Ca0. 4Sr0. 6-xNdxFe12. 0-x (Nb0. 5Zn0. 5) xO19. 2018. **765**: p. 616-623.

Yang, Y., et al., Effects of Pr-Al co-substitution on the magnetic and structural properties of M-type Ca-Sr hexaferrites. 2020. **63**: p. 337-347.

Junaid, M., et al., Structural, spectral, dielectric and magnetic properties of indium substituted copper spinel ferrites synthesized via sol gel technique. 2020. **46**(17): p. 27410-27418.

Kambale, R., et al., Dielectric properties and complex impedance spectroscopy studies of mixed Ni–Co ferrites. 2009. **18**(8): p. 085014.

Gholizadeh, A. and M.J.P.B.C.M. Beyranvand, Investigation on the structural, magnetic, dielectric and impedance analysis of Mg0. 3-xBaxCu0. 2Zn0. 5Fe2O4 nanoparticles. 2020. **584**: p. 412079.

Alange, R., et al., Structural, magnetic and dielectrical properties of Al–Cr Co-substituted M-type barium hexaferrite nanoparticles. 2016. **1106**: p. 460-467.

Iqbal, M.J. and M.N.J.C.E.J. Ashiq, Physical and electrical properties of Zr–Cu substituted strontium hexaferrite nanoparticles synthesized by co-precipitation method. 2008. **136**(2-3): p. 383-389.

Junaid, M., et al., Impact of Bi–Cr substitution on the structural, spectral, dielectric and magnetic properties of Y-type hexaferrites. 2020. **46**(16): p. 25478-25484.

Iqbal, M.J., et al., Effect of doping of Zr–Zn binary mixtures on structural, electrical and magnetic properties of Sr-hexaferrite nanoparticles. 2009. **478**(1-2): p. 736-740.

Annual Methodological Archive Research Review
http://amresearchreview.com/index.php/Journal/about
Volume 3, Issue 10 (2025)

Online ISSN 3007-3197
Print ISSN 3007-3189

http://amresearchreview.com/index.php/Journal/about

Ali, I., et al., Effect of Eu–Ni substitution on electrical and dielectric properties of Co–Sr–Y-type hexagonal ferrite. 2014. **49**: p. 338-344.

Mahalakshmi, S., et al., Electrical properties of nanophase ferrites doped with rare earth ions. 2014. **27**(9): p. 2083-2088.

Asghar, G., M.J.J.o.a. Anis-ur-Rehman, and compounds, Structural, dielectric and magnetic properties of Cr–Zn doped strontium hexa-ferrites for high frequency applications. 2012. **526**: p. 85-90.

Chowdari, B. and R.J.S.S.I. Gopalakrishnan, AC conductivity analysis of glassy silver iodomolybdate system. 1987. **23**(3): p. 225-233.

Ashiq, M.N., et al., Structural, magnetic and dielectric properties of Zr–Cd substituted strontium hexaferrite (SrFe12O19) nanoparticles. 2009. **487**(1-2): p. 341-345.

Gul, I., A.J.J.o.A. Maqsood, and Compounds, Structural, magnetic and electrical properties of cobalt ferrites prepared by the sol–gel route. 2008. **465**(1-2): p. 227-231.

Lee, S.-w., et al., Synthesis and characterization of hard magnetic composite photocatalyst—Barium ferrite/silica/titania. 2006. **96**(2-3): p. 483-488.

Xu, J., et al., Influence of Nd3+ substitution on the microstructure and electromagnetic properties of barium W-type hexaferrite. 2010. **490**(1-2): p. 552-556.